A New Surface Discharge Source: Plasma Characteristics and Delivery of Reactive Species

Bingchuan Wang, Dingxin Liu, Zhiquan Zhang, Qiaosong Li, Xiaohua Wang, and Michael G Kong

***Abstract*— A new surface dielectric barrier discharge source containing a matrix of holes in the dielectric slice is put forward in this paper, for which the plasma characteristics and the delivery of reactive species to the downstream sample are studied for three experimental conditions, i.e., EC1 with a helium gas flow of 1 SLM through the holes, EC2 with an artificial air flow of 1 SLM, and EC3 without any gas flow. All the other conditions are kept the same. For the same discharge power of 2 W, it is found that the surface plasma in EC1 is comparatively more homogeneous, the discharge voltage is lower by ∼12%, and the densities of reactive species are much higher, since the emission spectral lines of N_2(C), N_2^+(B), He($3s^3$S), and O($3p^5$P) are stronger by at least sixfold. A petri dish of deionized water is put 5-mm downstream the surface discharge, in which the concentrations of nitrite, nitrate, H_2O_2, and NO are measured after the plasma treatment of 3 min. Compared with EC1, EC2, and EC3, it is found that the gas flow can increase the concentration of H_2O_2 by ∼1.4-fold, but when helium is participated, a further increase of sixfold is achieved. Similarly, further increase is also found for the other three reactive species, which may be ascribed to the higher densities of gaseous reactive oxygen and nitrogen species in the helium-participated plasma and their larger diffusion coefficients in helium compared with that in air.**

***Index Terms*— Characteristics, delivery, surface dielectric barrier discharge (DBD).**

I. Introduction

DIELECTRIC barrier discharges (DBDs) are one of the most common sources for generating cold plasma, of which a special structure, namely, surface DBD, is intensively studied in recent years [1]–[8]. Surface DBD normally consists of a dielectric slice sandwiched between the high-voltage (HV) and grounded electrodes, and at least one electrode has a mesh or strip structure [1]–[8]. This structure allows plasmas be generated on the dielectric surface in the mesh and/or strip area, which has several application advantages, including ambient air operation, near room temperature, and macroscopically homogeneous plasma over a large surface area of hundred square centimeters [9]–[12]. Therefore, surface DBD has great potential for various applications, such as biomedicine [1], [5], [13], environmental protection [3], [8], and airflow control [2], [7].

Surface DBD in open air can generate various kinds of reactive species, especially the reactive oxygen and nitrogen species (RONS), which are deemed to play a dominant role in the biomedical applications [14], [15]. However, the nature of air, such as high breakdown voltage, low thermal conductivity, and high electronegativity, limits the yield of RONS in room temperature, which restricts the application efficiency of the surface discharge. Moreover, the sample that to be treated is normally located millimeters to centimeters away from the surface plasma, and hence some plasma-generated RONS have low possible to reach the sample due to their short lifetimes. For example, the diffusion distance during lifetime of OH is less than 1 mm in air [4]. Therefore, besides the yield of RONS, the delivery of them from the surface discharge to the downstream sample is also crucial for the applications. This motivates us to modify the conventional surface DBD structure to overcome the above application restrictions.

In this paper, a new surface discharge source is presented. Compared with the conventional sources for surface DBD, a matrix of small holes exists in the dielectric slice, which allows a weak gas flow through it. The helium gas flow decreases the discharge voltage, increases the plasma homogeneity, and also increases the densities of gaseous RONS as well as the delivery of them to the downstream sample, making the surface discharge more suitable for various applications.

This paper is organized as follows. The experimental setup is described in Section II. The experimental results including the electrical characteristics, the emission spectra of the plasmas, and the concentrations of the RONS in the downstream water, are presented and discussed in Section III. Finally, the conclusions are given in Section IV.

II. Experimental Methods

The schematic of the experimental setup used in this paper is shown in Fig. 1. The surface discharge source consists of

Manuscript received May 31, 2016; revised September 22, 2016; accepted October 19, 2016. This work was supported by the National Science Foundation of China, (Grant No.51307134 and 51521065, and also the Fundamental Research Funds for the Central Universities and the State Key Laboratory of Electrical Insulation and Power Equipment (Grant No.EIPE14129).

B. Wang, D. Liu, Z. Zhang, Q. Li, and X. Wang are with the State Key Laboratory of Electrical Insulation and Power Equipment, Center for Plasma Biomedicine, Xi'an Jiaotong University, Xi'an 710049, China (e-mail: liudingxin@mail.xjtu.edu.cn).

M. G. Kong is with the State Key Laboratory of Electrical Insulation and Power Equipment, Center for Plasma Biomedicine, Xi'an Jiaotong University, Xi'an 710049, China, also with the Frank Reidy Center for Bioelectrics, Old Dominion University, Norfolk, VA 23508 USA, and also with the Department of Electrical and Computer Engineering, Old Dominion University, Norfolk, VA 23529 USA.

Color versions of one or more of the figures in this paper are available online at http://ieeexplore.ieee.org.

Digital Object Identifier 10.1109/TPS.2016.2620565

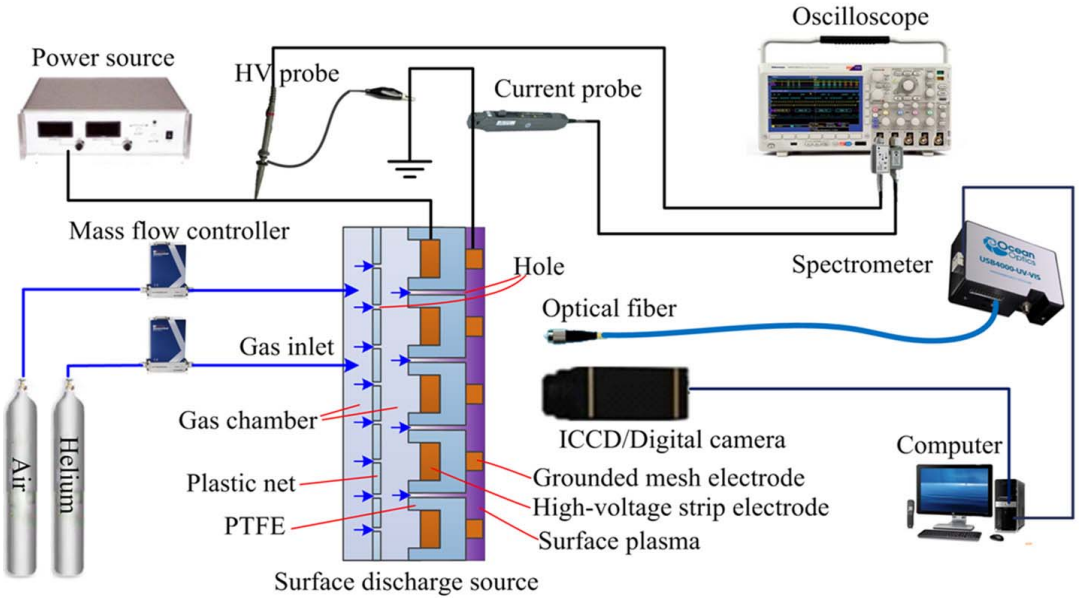

Fig. 1. Schematic of the experimental setup.

a gas chamber, a series of strip electrodes connecting to an HV power source, a grounded mesh electrode, a uniform flow orifice, and a dielectric slice sandwiched between the HV and grounded electrodes, which is made of polytetrafluoroethylene. A matrix of small holes exists in the dielectric slice to allow gas flowing through it, and entrance steps exist around the holes in the gas chamber to avoid the possible surface flashover. A uniform flow orifice is located between the gas inlet and the outlet holes to make the gas flow more uniform among the holes. Totally, five copper strips are used as the HV electrode, each of which has a size of 66 × 2 × 2 mm (length × height × width), and each mesh element of the grounded electrode has a hexagon shape with each side 4 mm in length, 0.76 mm in width, and 0.5 mm in thickness. The separation between the HV and grounded electrodes is 1.2 mm. Totally, 31 holes exist in the dielectric slice with the same diameter of 0.8 mm. As shown in Fig. 2, each hole locates at the center point of each mesh element, and on the other side of the dielectric slice, it locates in the middle position between two adjacent strip electrodes. The electrode structure of the surface discharge source has, to the best of our knowledge, never been reported before. An electrode structure reported by Sakai *et al*. [16] is similar to have mesh electrodes with gas flow through the mesh holes, but the mesh hole size is just ∼200 μm, so microhollow discharge is generated. Instead, here the discharge is a typical surface discharge as will be discussed in the following.

A sinusoidal voltage with a frequency of 20 kHz was applied on the HV electrode. The discharge voltage was measured by an HV probe (Tektronix, P6015A), of which the delay time is 14.7 ns and the bandwidth is 75 MHz. The discharge current was measured by a current probe (Tektronix, P6021), of which the delay time is 9.0 ns and the bandwidth is 450 Hz–60 MHz. The voltage and current waveforms were recorded by a digital oscilloscope (Tektronix, DPO3000) with a bandwidth

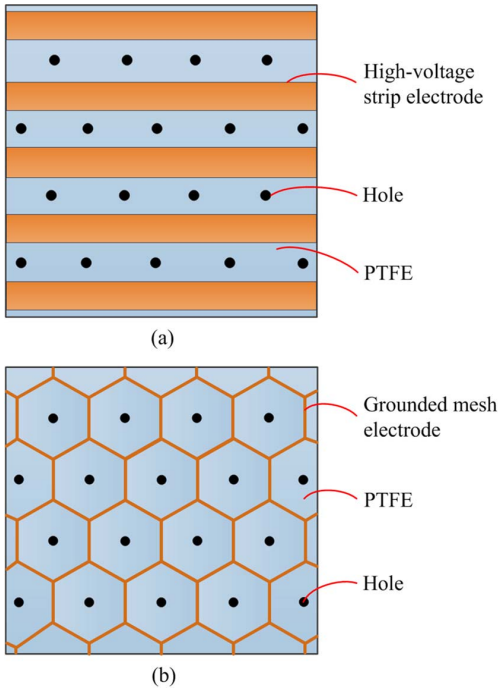

Fig. 2. Partial views of (a) HV side and (b) grounded side of the electrodes.

of 500 MHz. The discharge power was then obtained based on the time integration of the voltage and current waveforms over one cycle, and the delay time differences of the two probes were eliminated before the integration.

Three experimental conditions were studied for the gas flow through the holes, namely, EC1 with a helium (5N) gas flow of 1 SLM, EC2 with an artificial air flow of 1 SLM, and EC3 without any gas flow. The artificial air contains vol.79% N_2 and vol.21% O_2 with 99.99% purity.

In EC1 and EC2, the gas flow rate through each hole is just ~32.3 sccm (1 SLM/31 holes). A comparative study on the plasma characteristics and the delivery of reactive species was made for these conditions, of which the discharge power was kept the same to be 2 W.

The plasma images were taken either by a digital camera (Nikon, D7000) with an exposure time of 0.4 s, or by an ICCD camera (Princeton Instruments, PI-MAX3) with much shorter exposure time of 100 ns. The images taken by ICCD can demonstrate the spatial evolution of the plasmas in a cycle of the applied voltage. The emission spectra of the plasmas were detected by a spectrometer (Ocean Optics, USB2000) with an integral time of 3 min. In order to study the influence of gas flow on the gas temperature of the plasmas, a thermocouple probe is used to measure the temperature of the grounded mesh electrode after the plasma-on time of 3 min.

In order to study the delivery of reactive species to the downstream sample, a petri dish of deionized water (1 mL) was put 5 mm underneath the surface discharge source, and the concentrations of H_2O_2, nitrite (HNO_2/NO_2^-), and nitrate (HNO_3/NO_3^-) were measured by using a microplate reader (Thermo Scientific, Varioskan Flash Reader). The Amplex Red reagent was added into the water right after the plasma treatment of 3 min, and it reacted with H_2O_2 in a 1:1 stoichiometry to produce the red-fluorescent oxidation product, which was excited at $\lambda = 550$ nm and emitted at $\lambda = 595$ nm. Similarly, the Griess reagent was added into the water to detect nitrite, and the absorbance was measured at $\lambda = 540$ nm. A nitrate reductase enzyme was added into the water in company with the Griess reagent, in which case the nitrate would transform to nitrite, and therefore the absorption spectral at $\lambda = 540$ nm reflects the total concentration of nitrite and nitrate. The concentration of nitrate was then obtained by subtracting the nitrite concentration from the total concentration of nitrate and nitrite, similar to those reported in the literature [1], [4]. Moreover, the aqueous NO was also measured by an *X*-band electron spin resonance (ESR) equipment (BrukerBioSpin GmbH, EMX) after plasma treatment of 3 min. N-(Dithiocarbamoyl)-N-methyl-D-glucamine, sodium salt (MGD) was used as the spin trapping reagent, which was added into the water prior to the plasma treatments. It reacts with NO to produce the stable spin adduct with a peak intensity ratio of 1:1:1. The ESR measurement was performed according to the manufacturer's protocol, as did in [17]. All measurements were repeated three times.

III. Results and Discussion

A. Discharge Characteristics

The discharge images taken by the digital camera are shown in Fig. 3(a) and (b) for the discharge conditions EC1 and EC2, respectively. The discharge image of EC3 is very similar to that of EC2, and hence not shown here. It is noted that only partial area of the surface plasmas is shown in Fig. 3. Totally, 31 mesh elements are ignited for all the three experimental conditions, covering an area of ~17.16 cm^2.

As shown in Fig. 3, both images have good mesh-to-mesh homogeneities, but in comparison, their patterns are much different. In particular, the image pattern of EC1 has a brightest center in each mesh element, but for EC2 nearly no emission is observed there. This may be attributed to: 1) the breakdown strength of helium is lower than of air by several times [18] and 2) the special electrode structure which makes the electric field larger in the edge region of a mesh than that in the center part [19]. The gaps between two adjacent HV strip electrodes on the other side of the dielectric slice [see Fig. 2(a)] inhibit the plasmas to be generated on the opposite surface area, resulting in strips of nondischarge areas in EC2 [Fig. 3(b)]. By contrast, nearly the whole area of each mesh is covered by plasma in EC1 [Fig. 3(a)]. So, helium gas flow makes the surface plasma much more homogeneous in macroscale (the exposure time is 0.4 s). Considering that the plasma covers an area of ~19.7 cm^2, the gas flow rate of helium is very low, i.e., ~50.7 sccm/cm^2. This gas consumption is much lower than that for a plasma jet array with similar plasma area of section [20], and therefore providing a cheaper method for large-area plasma treatment.

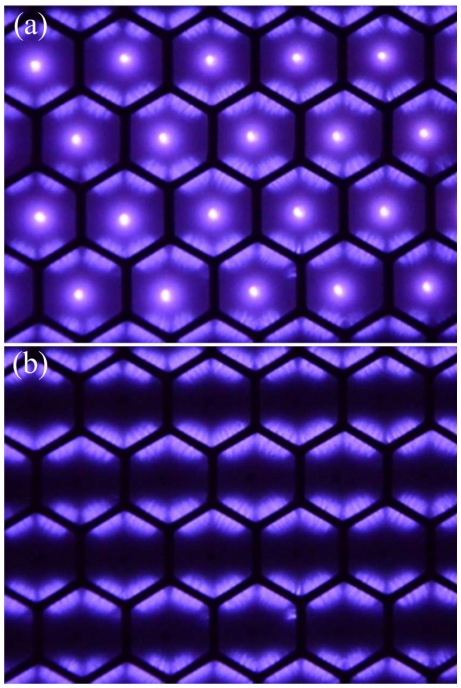

Fig. 3. Discharge images taken by the digital camera under the conditions of (a) EC1 and (b) EC2. (Exposure time is 0.4 s.)

The spatiotemporal evolutions of the surface plasmas in a single mesh in EC1 and EC2 are plotted in Fig. 4, in company with the corresponding discharge voltage and current waveforms. Again, it is noted that the time-resolved discharge images of EC3 are also similar to that of EC2, and hence not shown here. The discharge voltage has a peak-to-peak value of 8.8 kV in EC2 [see Fig. 4(b)], but it decreases to 7.7 kV in EC1 [Fig. 4(a)] due to the presence of helium. More burrs exist in the current waveform of EC1, which may also because helium is easier to breakdown.

As shown in Fig. 4, the evolutions of image patterns are much different for the two experimental conditions. Four main discharges happen in each cycle of the applied voltage in EC1,

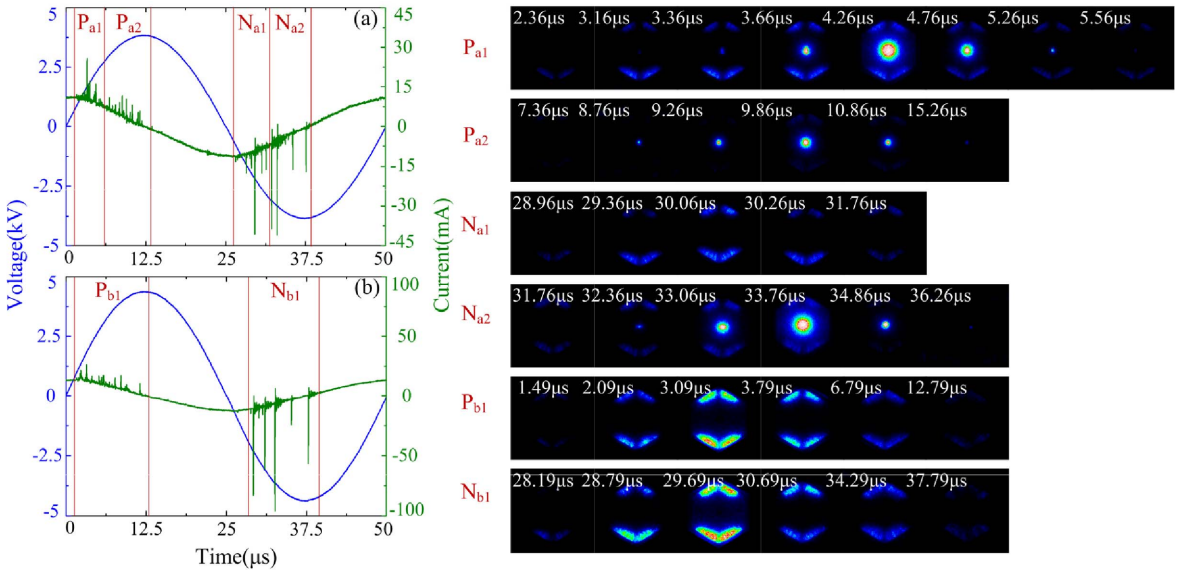

Fig. 4. Waveforms of the discharge voltage and current under the conditions of (a) EC1 and (b) EC2, as well as the corresponding time-resolved discharge images of a single mesh in the temporal regions of P_{a1}, P_{a2}, N_{a1}, N_{a2}, P_{b1}, and P_{b2}. The boundaries of the temporal regions are marked in (a) and (b) with red lines in a voltage cycle, while the instants for photographing are provided in each discharge image. The exposure time for the images is 100 ns.

i.e., in the temporal regions P_{a1} and P_{a2} for the positive half cycle, as well as N_{a1} and N_{a2} for the negative half cycle. In the temporal region P_{a1}, the discharge occurs in the edge region of the mesh element at the instant of ~2.36 μs, and then, it also happens in the center part at ~3.16 μs. The circular pattern in the center part expands till ~4.26 μs and then shrinks, while on the other hand, the luminous pattern in the edge region changes a little from ~3.16 to ~4.76 μs. The luminous patterns in the center part and in the edge region disappear simultaneously at ~5.56 μs, indicating the cease of the first discharge. The second discharge in P_{a2} occurs at ~1.8 μs latter, which also originates in the edge region. Both the luminous patterns in the center part and in the edge region expand first and then shrink, and the luminous pattern in the edge region disappears in prior to that in the center part. Compared with the first discharge, the luminous patterns are much weaker especially for that in the edge region. However, the second discharge lasts from ~7.36 to 15.26 μs, more than twofold longer than the first one. The third discharge occurs at ~28.96 μs in the negative half cycle, and ceases at ~31.76 μs. Interestingly, no luminous pattern is observed in the center part. The luminous pattern emerges again in the last discharge, which is more brighter and lasts more time compared with the third one. It can be seen from the discharge images of EC1 that the plasma covers nearly the whole mesh area around 4.26 μs in P_{a1} and 33.76 μs in P_{a2}.

Different to EC1, only two main discharges (P_{b1} and N_{b1}) happen in EC2 either in the positive or negative half cycle. Without the presence of helium, the luminous patterns for both discharges are confined in the edge region of the mesh element, lasting for around 10 μs before they disappear. The luminous patterns have similar evolution characteristics, but in comparison, the discharge in negative half cycle is slightly stronger.

The emission spectra of the surface plasmas in EC1 and EC2 are shown in Fig. 5. The plasma emission spectrum of

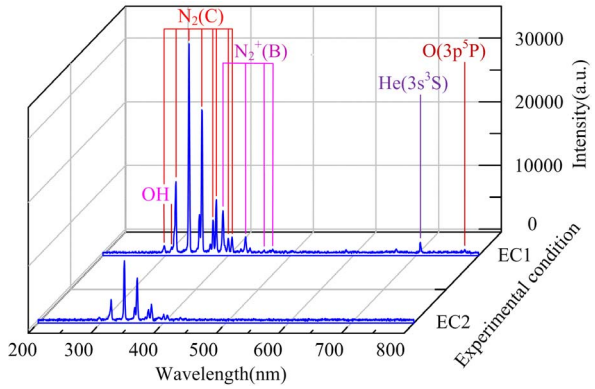

Fig. 5. Emission spectra of the surface plasmas for EC1 and EC2.

EC3 is similar to that of EC2, and hence not shown here. Only the emission lines of OH(A), N_2(A), and N_2^+(C) are observed for EC2, but for EC1, the emission lines at 706 nm [$He(3s^3S) \rightarrow He(2p^3P)$] and 777 nm [$O(3p^5P) \rightarrow O(3s^5S)$] are also observed. Moreover, the emission lines of OH(A), N_2(C), and N_2^+(B) have their intensities increase with the presence of helium, e.g., the spectral line of OH(A) at 308.9 nm increases by 13.5-fold, the spectral line of N_2(C) at 337 nm increases by sixfold, and the spectral line of N_2^+(B) at 391 nm increases by 29.1-fold. Given that the emission intensity is proportional to the density of the corresponding excited species, its increase indicates that the surface plasma in EC1 is much more efficient for the production of excited reactive species.

Considering the large area of the surface plasma, the gas flow of helium is very weak (~50.7 sccm/cm^2), so intuitively, it is so strange that the production efficiency of reactive species can be increased such much. However, the thickness of the discharge is approximately 100 nm on the dielectric surface [21], where the helium has not yet been well diluted by the open air. Furthermore, the plasmas in EC1 (see Fig. 4)

are mainly generated around the holes, where the helium concentration must be high. With the presence of helium, more electrons can be generated by the Penning ionization, and consequently, the generation rate of those excited species is enhanced [22]. On the other hand, the quenching rate of excited species in helium is much lower than that in air, which also leads to higher densities of excited species in EC1 [23]. So, the plasma characteristics are changed significantly by the relatively weak gas flow of helium.

Helium gas flow also has an advantage of inhibiting the gas temperature rise of the plasma, which can be reflected by the temperature rise of the grounded mesh electrode. After the plasma-on time of 3 min, the temperature rise of the mesh electrode is ∼1.8 K for EC1, while it is ∼2.5 K for EC2 and ∼4.6 K for EC3. The difference between EC2 and EC3 should be attributed to the gas flow, and for the further decrease of the gas temperature rise in EC1, it should be because the thermal conductivity of helium is larger than that of air. From the application point of view, the plasmas in EC1 have the lowest temperature rise during a whole plasma treatment procedure, and hence benefit the temperature sensitive applications, such as plasma biomedicine.

B. Delivery of Reactive Species to the Downstream Sample

For the applications of surface discharge, the sample to be treated is normally located in the downstream region millimeters to centimeters away from the plasma, and hence it is of importance to efficiently deliver the plasma-generated reactive species, especially for the RONS, to the sample. Compared with the three experimental conditions, the gas flows in EC1 and EC2 benefit for delivering the reactive species, and the presence of helium is also a favorable factor, since the diffusion coefficient of reactive species is larger in helium than that in air. For example, the diffusion coefficient of OH in atmospheric-pressure helium is 0.87 cm^2/s, but in air, it is just 0.21 cm^2/s [24]. In order to quantify the effect of the air gas flow (EC2 versus EC3) and the presence of helium (EC1 versus EC2) on the delivery of RONS, a petri dish of deionized water was put 5 mm underneath the surface discharge source, and the concentrations of long-lived species, including H_2O_2, nitrite, and nitrate, as well as the short-lived species NO were measured and then compared for the three experimental conditions.

As shown in Fig. 6, the measured concentration of H_2O_2 for EC3 is 3.83 μm, it increases by 1.37-fold due to the air flow of 1 SLM (EC2), and further increases by sixfold due to the presence of helium (EC1). This trend is also true for nitrite and nitrate, and the increments for all the three species from EC3 to EC2 are similar, but the increments from EC2 to EC1 are much different. For example, the increment of nitrite concentration from EC2 to EC1 is just 1.27-fold, more than four times lower than that for H_2O_2. As discussed above, the plasma characteristics change a little by the air flow, so the air flow increases the delivery of RONS mainly by advection, which is the same for all the three species. This may be why the differences of their concentrations in EC2 and EC3 are similar. On contrast, the presence of helium in EC1 changes the plasma

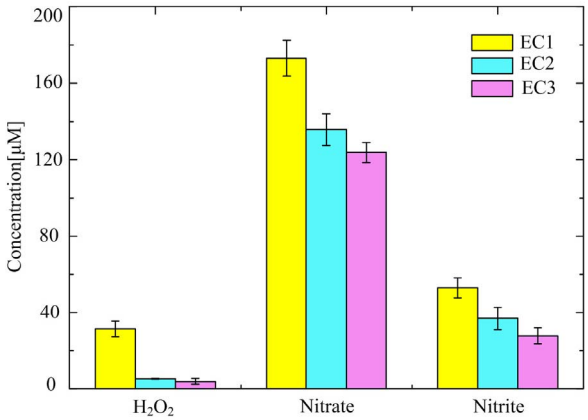

Fig. 6. Concentrations of H_2O_2, nitrate, and nitrite in deionized water for EC1, EC2, and EC3 after plasma treatment time of 3 min.

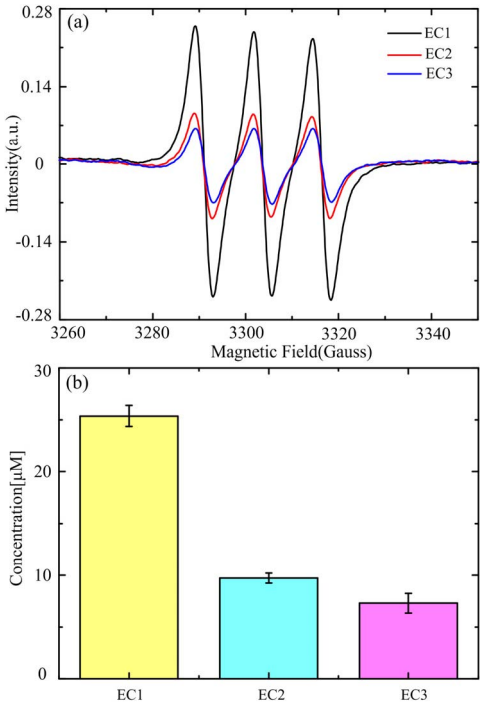

Fig. 7. (a) ESR spectra of the spin adduct of NO and (b) its concentrations for EC1, EC2, and EC3, respectively.

characteristics greatly, especially for the densities of gaseous reactive species, and hence influences the delivery amount of reactive species to the downstream water. The change in the densities of RONS should be different for different species, and hence the increments from EC2 to EC1 are different among each other.

NO is chosen as a representative to study the influence of helium gas flow on the delivery of short-lived species. Although the water is 5 mm away from the surface plasmas, the aqueous NO can be detected by ESR for all the three experimental conditions. As shown in Fig. 7(a), each of the ESR spectra has three characteristic peaks with an intensity ratio of 1:1:1, demonstrating the existence of NO in the plasma treated water [12]. The concentrations of the spin adduct are shown in Fig. 7(b) for EC1, EC2, and EC3, respectively.

These concentrations represent the relative values of that for aqueous NO, rather than the absolute values. This is because the spin adduct has much longer lifetime than the original free radical, and hence can accumulate to a relatively large concentration to be detected by ESR [25]. It can be seen from Fig. 7(b) that the concentration of NO increases by 1.3-fold from EC3 to EC2, similar to that for the long-lived species. The increment from EC2 to EC1 is about 2.6, suggesting that the presence of helium also benefits for the delivery of short-lived species. It should be noted that the aqueous NO may not be diffused from the gas phase, instead it may be generated *in situ* in the plasma-activated water, but in the latter case, it is also generated by the other short-lived species originated from the gas phase [26].

From Figs. 6 and 7, it can be concluded that the helium gas flow can greatly increase the delivery of RONS to the downstream sample, although the flow rate is very weak. This is partially attributed to the gas flow itself, which leads to ∼1.4-fold increment, and also attributed to the gain in densities of RONS in the surface discharge as well as the increase of diffusion coefficient in helium-mixed gas gap between the discharge and the water.

IV. Conclusion

A new surface discharge source is put forward in this paper, which consists of several HV strip electrodes, a grounded mesh electrode, and a dielectric slice sandwiched between the HV and the grounded electrodes. The dielectric slice has many small holes of 0.8 mm diameter, which is located at the center point of each mesh element, while on the other side of the slice, they are in the middle position between two strip electrodes.

Three experimental conditions are studied for comparison, i.e., EC1 with a helium gas flow of 1 SLM, EC2 with an artificial air flow of 1 SLM, and EC3 without any gas flow. All the other conditions are kept the same. Helium gas flow is only 32.3 sccm per each holes (∼50.7 sccm/cm^2 of the plasma), but it changes the plasma characteristics greatly. It is found that the surface plasma is comparatively more homogeneous in EC1, because in that case, the gas content of helium is much higher in the center region of each mesh, and consequently the gas breakdown can happen there although the electric field is lower than that in the edge region. For the same discharge power of 2 W, the peak-to-peak value of discharge voltage in EC1 is comparatively lower by 1.1 kV, but the densities of reactive species are much higher, since the intensities of emission spectral lines of N_2(C), N_2^+(B), He($3s^3$S), and O($3p^5$P) are stronger by at least sixfold.

The delivery of reactive species to the treated sample is studied by putting a petri dish of deionized water in the downstream region 5 mm away from the surface plasma. After plasma-on time of 3 min, the concentrations of nitrite, nitrate, H_2O_2, and NO in the water are measured for the three experimental conditions. It is found that the gas flow can increase the concentration of H_2O_2 by only 1.4-folds (EC2 versus EC1), but when helium is participated, a further increase of sixfold is achieved (EC1 versus EC2). This further increase is also true for the other three reactive species, especially for NO, which has a very short lifetime in gas phase. In principle, it may be ascribed to the higher densities of gaseous RONS in the helium-participated plasma and the larger diffusion coefficients in helium compared with that in air.

References

[1] V. Boxhammer *et al.*, "Bactericidal action of cold atmospheric plasma in solution," *New J. Phys.*, vol. 14, no. 11, p. 113042, 2012.

[2] Y. Wu *et al.*, "Influence of operating pressure on surface dielectric barrier discharge plasma aerodynamic actuation characteristics," *Appl. Phys. Lett.*, vol. 93, no. 3, p. 031503, 2008.

[3] T. Shibata and H. Nishiyama, "Numerical study of chemical reactions in a surface microdischarge tube with mist flow based on experiment," *J. Phys. D, Appl. Phys.*, vol. 47, no. 10, p. 105203, 2014.

[4] Z. C. Liu *et al.*, "Physicochemical processes in the indirect interaction between surface air plasma and deionized water," *J. Phys. D, Appl. Phys.*, vol. 48, no. 49, p. 495201, 2015.

[5] M. J. Pavlovich, H.-W. Chang, Y. Sakiyama, D. S. Clark, and D. B. Graves, "Ozone correlates with antibacterial effects from indirect air dielectric barrier discharge treatment of water," *J. Phys. D, Appl. Phys.*, vol. 46, no. 14, p. 145202, 2013.

[6] D. Li, D. X. Liu, Q. Y. Nie, H. P. Li, H. L. Chen, and M. G. Kong, "Array of surface-confined glow discharges in atmospheric pressure helium: Modes and dynamics," *Appl. Phys. Lett.*, vol. 104, no. 20, p. 204101, 2014.

[7] A. Cristofolini, C. A. Borghi, and G. Neretti, "Charge distribution on the surface of a dielectric barrier discharge actuator for the fluid-dynamic control," *J Appl. Phys.*, vol. 113, no. 14, p. 143307, 2013.

[8] P. Olszewski, J. F. Li, D. X. Liu, and J. L. Walsh, "Optimizing the electrical excitation of an atmospheric pressure plasma advanced oxidation process," *J. Hazardous Mater.*, vol. 279, pp. 60–66, Aug. 2014.

[9] M. Šimor, J. Ráhel, P. Vojtek, M. Čemák, and A. Brablec, "Atmospheric-pressure diffuse coplanar surface discharge for surface treatments," *Appl. Phys. Lett.*, vol. 81, no. 15, pp. 2716–2718, 2002.

[10] J. Pons, E. Moreau, and G. Touchard, "Asymmetric surface dielectric barrier discharge in air at atmospheric pressure: Electrical properties and induced airflow characteristics," *J. Phys. D, Appl. Phys.*, vol. 38, no. 19, pp. 3635–3642, 2005.

[11] J. M. Williamson, D. D. Trump, P. Bletzinger, and B. N. Ganguly, "Comparison of high-voltage AC and pulsed operation of a surface dielectric barrier discharge," *J. Phys. D, Appl. Phys.*, vol. 39, no. 20, pp. 4400–4406, Oct. 2006.

[12] S. Pekárek, "Experimental study of surface dielectric barrier discharge in air and its ozone production," *J. Phys. D, Appl. Phys.*, vol. 45, no. 7, p. 075201, 2012.

[13] S. Y. Zhong *et al.*, "Surface air plasma-induced cell death and cytokine release of human keratinocytes in the context of psoriasis," *Brit. J. Dermatol.*, vol. 174, no. 3, pp. 542–552, 2015.

[14] M. G. Kong *et al.*, "Plasma medicine: An introductory review," *New J. Phys.*, vol. 11, no. 11, p. 115012, 2009.

[15] D. B. Graves, "The emerging role of reactive oxygen and nitrogen species in redox biology and some implications for plasma applications to medicine and biology," *J. Phys. D, Appl. Phys.*, vol. 45, no. 26, p. 263001, 2012.

[16] O. Sakai, Y. Kishimoto, and K. Tachibana, "Integrated coaxial-hollow micro dielectric-barrier-discharges for a large-area plasma source operating at around atmospheric pressure," *J. Phys. D, Appl. Phys.*, vol. 38, no. 3, pp. 431–441, 2005.

[17] H. Tresp, M. U. Hammer, J. Winter, K.-D. Weltmann, and S. Reuter, "Quantitative detection of plasma-generated radicals in liquids by electron paramagnetic resonance spectroscopy," *J. Phys. D, Appl. Phys.*, vol. 46, no. 43, p. 435401, 2013.

[18] "Paschen's law," (Oct. 19, 2016) [Online]. Available: https://en.wikipedia.org/wiki/Paschen%27s_law

[19] N. Bednar, J. Matović, and G. Stojanović, "Properties of surface dielectric barrier discharge plasma generator for fabrication of nanomaterials," *J. Electrostatics*, vol. 71, no. 6, pp. 1068–1075, 2013.

[20] Q. Y. Nie, Z. Cao, C. S. Ren, D. Z. Wang, and M. G. Kong, "A two-dimensional cold atmospheric plasma jet array for uniform treatment of large-area surfaces for plasma medicine," *New J. Phys.*, vol. 11, no. 11, p. 115015, 2009.

[21] Y. Sakiyama, D. B. Graves, H.-W. Chang, T. Shimizu, and G. E. Morfill, "Plasma chemistry model of surface microdischarge in humid air and dynamics of reactive neutral species," *J. Phys. D, Appl. Phys.*, vol. 45, no. 42, p. 425201, 2012.

[22] J. L. Walsh, D. X. Liu, F. Iza, M. Z. Rong, and M. G. Kong, "Contrasting characteristics of sub-microsecond pulsed atmospheric air and atmospheric pressure helium–oxygen glow discharges," *J. Phys. D, Appl. Phys.*, vol. 43, no. 3, p. 032001, 2010.

[23] T. Murakami, K. Niemi, T. Gans, D. O'Connell, and W. G. Graham, "Chemical kinetics and reactive species in atmospheric pressure helium–oxygen plasmas with humid-air impurities," *Plasma Sour. Sci. Technol.*, vol. 22, no. 1, p. 015003, 2013.

[24] A. V. Ivanov, S. Trakhtenberg, A. K. Bertram, Y. M. Gershenzon, and M. J. Molina, "OH, HO_2, and ozone gaseous diffusion coefficients," *J. Phys. Chem. A.*, vol. 111, no. 9, pp. 1632–1637, 2007.

[25] B. Halliwell and M. Whiteman, "Measuring reactive species and oxidative damage *in vivo* and in cell culture: How should you do it and what do the results mean?" *Brit. J. Pharmacol.*, vol. 142, no. 2, pp. 231–255, 2004.

[26] D. X. Liu *et al.*, "Aqueous reactive species induced by a surface air discharge: Heterogeneous mass transfer and liquid chemistry pathways," *Sci. Rep.*, vol. 6, p. 23737, Apr. 2016.

Authors' photographs and biographies not available at the time of publication.